



HAL
open science

Hydrocarbon Fuels from Sequential Hydrothermal Liquefaction (HTL) of Lignite and Catalytic Upgrading of Crude Oil

Nuno Batalha, Ruben Checa, Chantal Lorentz, Pavel Afanasiev, Krzysztof Stańczyk, Krzysztof Kapusta, Dorothée Laurenti, Christophe Geantet

► **To cite this version:**

Nuno Batalha, Ruben Checa, Chantal Lorentz, Pavel Afanasiev, Krzysztof Stańczyk, et al.. Hydrocarbon Fuels from Sequential Hydrothermal Liquefaction (HTL) of Lignite and Catalytic Upgrading of Crude Oil. *Energy & Fuels*, 2024, 38 (2), pp.1019-1031. 10.1021/acs.energyfuels.3c04312 . hal-04433676

HAL Id: hal-04433676

<https://hal.science/hal-04433676v1>

Submitted on 22 Jul 2024

HAL is a multi-disciplinary open access archive for the deposit and dissemination of scientific research documents, whether they are published or not. The documents may come from teaching and research institutions in France or abroad, or from public or private research centers.

L'archive ouverte pluridisciplinaire **HAL**, est destinée au dépôt et à la diffusion de documents scientifiques de niveau recherche, publiés ou non, émanant des établissements d'enseignement et de recherche français ou étrangers, des laboratoires publics ou privés.

1 Hydrocarbon fuels from sequential hydrothermal liquefaction (HTL) of lignite
2 and catalytic upgrading of crude oil

3
4 *Nuno Batalha^{a*}, Ruben Checa^a, Chantal Lorentz^a, Pavel Afanasiev^a, Krzysztof Stańczyk^b, Krzysztof*
5 *Kapusta^b, Dorothée Laurenti^a, Christophe Geantet^a*

6 ^a Université de Lyon, Institut de Recherches sur la Catalyse et l'Environnement de Lyon (IRCELYON),

7 UMR5256 CNRS-UCB Lyon 1, 2 Avenue Albert Einstein, 69626, Villeurbanne Cedex, France

8 ^b Główny Instytut Górnictwa (Central Mining Institute), Plac Gwarków 1, 40-166 Katowice, Poland

9
10 * Corresponding Author: nuno.rocha-batalha@ircelyon.univ-lyon1.fr

11
12 **ABSTRACT**

13 Lignite from Belchatów in Poland was converted to hydrocarbon fuels, particularly in the kerosene
14 and diesel range, through sequential hydrothermal liquefaction (HTL) and hydrotreatment (HDT) of
15 the obtained crude oil. Different HDT temperatures were investigated (from 350°C up to 390°C).
16 Despite the highly aromatic nature and high heteroatom content, the HTL lignite crude oil could
17 undergo deep hydrodesulfurization (HDS = 99 %) and hydrodeoxygenation (HDO =98 %) in a single
18 HDT treatment stage, yielding a liquid product rich in aliphatic and aromatic, particularly
19 monoaromatic, hydrocarbons. The hydrotreatment and hydrogenating capacity of the lignite crude oil
20 was linked to the low concentration of compounds resistant to hydrotreatment in lignite and,
21 consequently, lignite's crude oil, permitting the easy transformation of the crude oil into hydrocarbon
22 fuel. Still, the significant concentration of aromatic compounds, particularly monoaromatic and
23 diaromatic, in the liquid product (≈45% of fuel range products) suggests further upgrading, blending,
24 or harsher HDT conditions might be necessary to improve the fuel quality.

25 In addition to the crude oil, the HTL of lignite yielded a stream of char, which displayed a higher
26 calorific value and lower heteroatom content than the original lignite feedstock, thus having a high
27 potential for electricity production, the common use of lignite. Thus, introducing an HTL stage to
28 extract crude oil before lignite use in electricity production could provide an alternative fuel source
29 used as a strategy to increase multiple countries' energetic independence.

30 Keywords: Lignite; hydrotreatment; Crude oil; liquid fuels; coal valorization

31 **1. INTRODUCTION**

32 The Russian invasion of Ukraine in February 2022 has redistributed the energetic policy in Europe
33 (and in the world) and deeply impacted the food and energetic markets and climate issues ¹. For
34 instance, the European Union (E.U.) is the first market for diesel fuel and must import 20% of its
35 consumption. Half of this imported diesel was coming from Russia. Despite E.U. policy attempts to
36 eliminate fossil resources, with a new target of 45% of renewables in 2030, energetic transition and
37 evolution of energetic policies are challenging to manage, and a portfolio of options must be
38 investigated. Biofuel production is expected to increase in the future². However, these are only
39 expected to cover 4.6% of transport fuel demand in 2024³. Therefore, there might be a need for a local
40 diesel resource in the E.U. before vehicles electrification and green fuels are fully implemented.

41 Despite its relatively low heat content, almost 80% of lignite is used for electricity generation⁴.
42 Even if its production has strongly decreased since the 90's in Europe, the inland consumption of
43 brown coal by E.U. member states was estimated, in 2021, at 300 Mt ⁵. An alternative pathway to
44 valorize lignite, pure or mixed with waste biomass, is hydrothermal liquefaction. In the absence of
45 oxygen, subcritical or supercritical water as a reaction medium converts organic matter,
46 independently of the origin, into a liquid of high heating value (HHV). In early works, Deshpande et al.,
47 Kershaw et al., and Hu et al. extracted brown coals or Dayan lignites, respectively, with sub and
48 supercritical water and claimed that the extraction residue would be a good feedstock for combustion
49 or gazification⁶⁻⁸. These studies led to the establishment of the hydrothermal dewatering (HTD)
50 process, a pretreatment (developed at pilot scale) of lignite with no particular address regarding the
51 crude oil formed ⁹. This was only tackled more recently by Hartman et al., which investigated the HTL
52 of selected coal feedstocks providing a high liquid yield (21%) and concluded that high-value
53 petroleum-like products could be obtained ¹⁰. Liu et al. used HTL as a pretreatment before pyrolysis
54 of Xiaolongtan lignite and suggested three reaction steps discussed hereafter¹¹. Like HTL of biomass,
55 numerous reactions occurring during HTL are favorable for deoxygenation and monomer formation,

56 even if condensation reactions may co-occur. Due to the complexity of the HTL process, the
57 optimization of operating conditions, i.e., the impact of lignite nature and the understanding of the
58 formation of the product, have yet to be deeply investigated. Recently, Li et al. attempted to optimize
59 HTL process parameters for the transformation of demineralized and pretreated lignite, observing
60 these can impact the liquid yield and composition¹². They also suggested that HTL promotes the
61 transfer from polycyclic aromatic hydrocarbons to monocyclic aromatic hydrocarbons. All these
62 studies indicate that HTL of lignite can potentially provide some fuel. However, no one attempted to
63 upgrade lignite HTL oil like it was done with the HTL biocrudes of biomass or wastes.

64 In the present work, we investigated the HTL conversion of a Polish lignite and the catalytic upgrading
65 of the HTL lignite oil obtained. A detailed study of the upgrading operating conditions and their impact
66 on the nature of the products was performed. After upgrading, a diesel fraction was obtained, showing
67 that a preliminary HTL stage can provide a fraction of a diesel source and increase the HHV of the
68 residue used for electricity generation.

69

70 **2. EXPERIMENTAL**

71 *2.1. Hydrothermal liquefaction of lignite*

72 Lignite from the coal mine of Bełchatów in Poland was used as feedstock. The physicochemical
73 characteristics of the feedstock are presented in Table 1. The HTL experiments were conducted in a
74 batch type 1000 ml stainless steel autoclave reactor (Autoclave Engineers, USA), equipped with a
75 magnetically coupled mechanical stirrer. In each of the HTL experiments, 600 g of 10 wt% of lignite in
76 water solution was used. After loading the reactor, the residual air was removed by nitrogen purging
77 and vacuuming four times. Subsequently, the vessel was pressurized with N₂ (~2 bar) and then heated
78 to 360 °C (reaction temperature) with a constant heating rate 10 °C/min and maintained at this
79 temperature for 30 min (HTL reaction time). The pressure in the reactor vessel was self-generated.
80 The experimental conditions used to perform the HTL are summarized in Table 2.

81 After completion of the reaction, the autoclave was cooled to ambient temperature, and the gas
82 samples were taken for analysis by micro-GC SRA instruments equipped with the following three
83 modules: MoSieve 5 Å with backflush, PoraPLOT U, and Plot Al₂O₃/KCl. The HTL products mixture

84 (crude oil, aqueous phase, and char) were then recovered from the reaction vessel. The separation of
 85 the products mixture obtained after the HTL processes was performed using a vacuum filtration
 86 technique. The post-reaction mixture was filtered on glass microfiber filters. The aqueous phase
 87 obtained was separated from the char. The reactor vessel and the char were washed with acetone,
 88 and the solid fraction and the liquid organic fraction (crude oil) solution in acetone were separated by
 89 vacuum filtration. Next, the solid fraction was dried to constant weight in the laboratory drying oven
 90 at 105 °C. The filtered crude oil solution was concentrated using a rotary vacuum evaporator. The
 91 scheme of the process is presented in Figure S1.

92 Table 1. Physicochemical properties of lignite feedstock.

Proximate Analysis	Moisture _{total} (wt.%) ^a	50.6
	Organic matter (wt.% dry) ^b	72.5
	Volatiles (wt.% dry) ^c	42.0
	Ash (wt.% dry) ^d	25.9
Ultimate analysis	C (wt.% dry)	50.5
	H (wt.% dry)	4.6
	N (wt.% dry)	0.6
	O (wt.% dry)	16.0
	S total (wt.% dry)	3.8
Calorific value _{as received} (kJ/kg)		8 130
Calorific value _{dry} (kJ/mol)		18 960

93 ^aWeight loss upon heating at 105°C (standard method: CEN/TS 15414-2:2010)

94 ^bWeight loss of dry sample upon combustion under air atmosphere (T = 550 °C). (Standard Method:
 95 PN-EN 15935:2013-02)

96 ^cWeight loss of dry sample under inert atmosphere (T=950 °C). (standard method: PN-G-04516:1998)

97 ^dWeight remaining after combustion of dry sample under air atmosphere (T=550 °C) (PN-EN
 98 15935:2013-02)

99

100

101 The yields of the products were calculated based on dry, ash-free (daf) initial lignite using the following
 102 formulas:

103

$$104 \text{ Crude oil yield (wt. \%)} = \frac{m_{\text{crude}}}{m_{\text{lignite}}} 100$$

Equation 1

105

106 $Char\ yield\ (wt.\ \%) = \frac{m_{char}}{m_{lignite}} 100$ Equation 2

107 $Gas\ yield\ (wt.\ \%) = \frac{\sum^i M_{w_i} y_i P V}{R T m_{Lignite}} 100$ Equation 3

108 $Aqueous\ phase\ solubles\ yield\ (wt.\ \%) = 100 - gas\ yield - char\ yield - crude\ oil\ yield$
 109 Equation 4

110

111 Where:

112 m_{crude} , m_{char} , and $m_{lignite}$ are the mass of recovered crude oil, recovered char, and initial lignite feedstock
 113 on a dry, ash-free (daf) basis;

114 M_{w_i} and y_i are the molecular weight and gas composition of compound i , respectively.

115 P is the residual reactor pressure at room temperature

116 V is the reactor volume occupied by gas (400 mL)

117 R , is the ideal gas constant

118 T , is the room temperature

119

120

121 Table 2. Summary of experimental conditions used for the hydrothermal liquefaction and
 122 hydrotreatment test.

Hydrothermal liquefaction (HTL)	
Feedstock	Lignite (Bełchatów, Poland)
Slurry concentration (wt.%)	10 (in water)
Batch volume (L)	0.6
Temperature (°C)	360
Reaction time (h)	0.5
Hydrotreatment (HDT)	
Feedstock	Lignite HTL crude oil
Feedstock mass (g)	3
Catalyst	NiMoS/P-Al ₂ O ₃
Catalyst mass (g)	1
Solvent	n-heptane
Solvent mass (g)	25
Reaction temperature (°C)	350, 375 and 390
Reaction time (h)	0, 1, and 3
Hydrogen pressure (bar)	10 (at room temperature) + 50 (at reaction temperature)

123

147 After the reaction, the reactor was cooled to room temperature, and the residual gas was collected in
 148 a gas bag and analyzed with a micro-GC (SRA instruments) equipped with three modules: Molsieve 5Å
 149 (H₂, CO, CH₄), Hayesep A (CO₂, C₂ hydrocarbons), PLOT Al₂O₃/KCl (C₃-C₄ hydrocarbons).

150 The liquid and all solids were separated through filtration and washing with heptane (≈ 100 mL). The
 151 heptane in the liquid was evaporated, using a rotovapor apparatus, for 2 h at a pressure of 30 mBar
 152 and a temperature of 40°C. The liquid remaining after evaporation was considered the liquid product
 153 from hydrotreatment. The solids recovered from filtration were dried at room temperature under a
 154 fumehood to remove the excess heptane. The total amount of solids produced in the reaction resulted
 155 from the difference between the dried solids and the fresh catalyst. Elemental analysis was used to
 156 determine the coke deposited in the catalyst, i.e., coke equivalent to carbon in the spent catalyst.

157 The yields of the products obtained from the hydrotreatment (HDT) reaction, i.e., liquid, solid, gas,
 158 H₂O, and H₂S were calculated through the following equations:

159
 160
$$\text{Liquid yield (wt. \%)} = \frac{m_{\text{liquid}}}{m_{\text{crude oil}}} 100 \quad \text{Equation 6}$$

161
 162
$$\text{solid yield (wt. \%)} = \frac{m_{\text{solid}}}{m_{\text{crude oil}}} 100 \quad \text{Equation 7}$$

163
$$\text{Gas yield (wt. \%)} = \frac{\sum^i M w_i y_i P V}{R T m_{\text{crude oil}}} 100 \quad \text{Equation 8}$$

164
$$H_2O \text{ (wt. \%)} = (O_{\text{crude oil}} - \text{Gas yield} \left(\frac{\%CO}{28} + 2 \frac{\%CO_2}{44} \right) 16 - \text{Liquid yield} \cdot O_{\text{liquid}}) \frac{18}{16} \quad \text{Equation 9}$$

165
$$H_2S \text{ (wt. \%)} = (S_{\text{crude oil}} - \text{Liquid yield} \cdot S_{\text{liquid}}) \frac{34}{32} \quad \text{Equation 10}$$

166
 167 Where:
 168 $m_{\text{crude oil}}$, m_{solid} , and m_{liquid} are, respectively, the mass of crude oil to be hydrotreated, the excess of
 169 mass found in the catalyst after reaction ($m_{\text{spent catalyst}} - m_{\text{fresh catalyst}}$), and the mass liquid obtained after
 170 evaporation of n-heptane;
 171 $M w_i$ and y_i are the molecular weight and gas composition of compound i, respectively.
 172 P is the residual reactor pressure at room temperature
 173 V is the reactor volume occupied by gas (≈ 263 mL)
 174 R, is the ideal gas constant
 175 T, is the room temperature

176 O, is the weight fraction of oxygen in the crude oil ($O_{\text{crude oil}}$) and liquid (O_{liquid}) determined by elemental
177 analysis.
178 %CO and %CO₂, are the weight fraction of CO and CO₂, respectively, in the gas
179 S, is the weight fraction of Sulfur in the crude oil ($S_{\text{crude oil}}$) and liquid (S_{liquid}).

180

181 2.3. Characterization methods

182 Elemental compositions (CHNS) of lignite, crude oil, hydrotreatment liquid, and spent catalyst were
183 analyzed on a Thermo Scientific FLASH 2000 Organic Elemental Analyzer (accuracy of ± 0.1 wt%). The
184 samples' oxygen (O) composition was also determined by elemental analysis with the same equipment
185 used for CHNS quantification but by using an alternative method specifically dedicated to oxygen
186 quantification. Additionally, the S composition of the crude oil and hydrotreatment liquid samples
187 were also quantified using ANTEK 9000NS apparatus, which is more sensitive (from few ppm until
188 percent levels) and accurate. Prior to analysis, the samples were diluted in THF (≈ 5 wt%).

189 The boiling point of the sulfur-containing compounds in the crude oil was estimated by using a Agilent
190 7890A GC coupled with an FPD+ detector and fitted with a CP-SimDist GC column (10 m \times 0.53mm \times
191 2.65 μ m).

192 The molecular weight distribution of the compounds in the lignite crude oil and the hydrotreatment
193 liquid was obtained by size exclusion chromatography (SEC) performed using an Agilent 1200 series
194 HPLC equipped with two PLgel Columns (50 and 500 \AA), a refractive index detector (RID), and a diode
195 array detector (DAD). The analysis was carried out at 35 $^{\circ}\text{C}$ using tetrahydrofuran (THF – 1 mL/min) as
196 the eluent. Before analysis, the samples were diluted to a concentration of ≈ 1 wt.% in THF and filtered
197 (0.45 μ m). A mixture composed of hydrocarbons (Mw from 86 to 1000 g/mol) was used as standard
198 to convert elution time into molecular weight (hydrocarbons equivalent) leading to an average MW_{HC}
199 data.

200 The ¹³C-NMR analysis of the liquid samples was performed in a Bruker AVANCE 400 MHz spectrometer
201 and analyzed using the software TopSpin 3.0. The measurements were performed at room
202 temperature with an accumulation of 4700 scans, with a relaxation time of 10 s, for approximately 15
203 h. The samples (≈ 100 mg) were diluted with deuterated chloroform (CDCl₃) (0.6 mL). Table S2 includes
204 the chemical shifts attributed to each functional group.

205 Comprehensive GC \times GC-TOF MS and GC \times GC-FID were used to identify and quantify the compounds in
206 the lignite crude oil and HDT liquid. The GC \times GC/TOF system was equipped with a cryogenic modulator

207 from Zoex Corporation (USA) and a BenchTOF 2 TI spectrometer from Sepsolve. The chromatograph
208 and TOF parameters are described in Tables S3 and S4. The GC×GC/FID was equipped with a switch
209 valve modulator (Agilent G3486A CFT modulator), and modulation parameters were optimized
210 according to ref ¹³. The parameters used for product separation are described in Table S3. The
211 quantification of the compounds detected by GC×GC-FID was performed using the relative responsive
212 factor method (RRF)¹⁴ with cyclohexanol as the reference. The data obtained from comprehensive
213 GC×GC-FID was also used to provide the distillation curve of the HDT liquid products by using a mixture
214 of n-alkanes (C₇ to C₄₀) as a reference.

215

216 **3. RESULTS AND DISCUSSION**

217 ***3.1. Hydrothermal liquefaction of lignite***

218 ***3.1.1. Crude oil***

219 While the primary target product for liquid fuel production is crude oil, only 12.3 wt.%daf of lignite
220 was transformed into this product with char (48.8 wt.%daf), gas (23wt.% daf), and aqueous phase
221 organics (15.9 wt.%daf) representing the main fractions. Liu et al. ¹⁵ studied the optimal conditions for
222 maximizing crude oil yield from lignite HTL and found that short residence times, i.e., ~5 min, and high
223 temperatures, i.e., ~400 °C, are necessary. In this study¹⁵, the authors found a maximum crude yield
224 of 34 wt.%. Hence, the high residence time (30 min) and low temperature (360 °C) presently used can
225 explain the low crude oil yield. Another important parameter known to affect the yield and quality of
226 crude oil in HTL is the amount of ash ^{16–20}. On biogenic feedstocks, such as algae, high ash contents
227 have been reported to decrease the yield and quality of the crude product ^{16–18}. Although no reference
228 applied to the conversion of lignite under HTL conditions was found, a direct analogy with biomass
229 feedstocks suggests that high-ash in lignite might have a similar effect. Thus, a high concentration of
230 ash found in lignite (25.94 wt.%) could also be responsible for the low crude oil yield (12.3 wt.%).
231 Indeed, Liu et al. ¹⁵ used lignite with 7.14 wt.% of ash. It should be mentioned that Oner et al.
232 demonstrated that ash positively enhances the crude oil product in lignite liquefaction under organic
233 solvents, like tetraline, and under H₂ pressure ²¹. However, the positive effects were attributed to the

234 capacity of certain elements in ash to promote hydrogenation by H₂ or hydrogen transfer from the
235 solvent, a reaction not likely to occur under HTL conditions. While ash is bound to affect lignite HTL
236 conversion, the chemical composition of lignite and lignite's ash is substantially different from that of
237 biomass feedstocks^{22,23}. Thus, further studies, out of the scope of this work, should be performed to
238 infer the impact of this component.

239 When compared to the lignite feedstock, the crude oil stream contains a higher concentration of
240 carbon (77.7 wt.% vs. 50.5 wt.%dry) and hydrogen (8.9 wt.% vs.4.6 wt.%dry) (Tables 1 and 2).
241 Additionally, the crude oil displayed a lower concentration of oxygen (10.8 wt.% vs. 16.0 wt.%dry) and
242 sulfur (2.4 wt.% vs. 3.78 wt.%dry) than the parent lignite sample. However, it is essential to mention
243 that the sulfur content in crude oil is still well above the specifications for liquid hydrocarbon fuels,
244 e.g., diesel specification < 10 ppm. Thus, significant desulfurization must take place during upgrading.
245 In the case of nitrogen, no specification states a maximum N concentration in hydrocarbon fossil
246 fuels²⁴. Still, nitrogen compounds impact other regulated properties, such as gum content, storage
247 stability, and thermal stability²⁵. However, synthetic aviation fuels (SAF) must have a nitrogen
248 concentration inferior to 2 ppm²⁶. It is worth mentioning that there is still no regulation concerning
249 HTL-derived fuels.

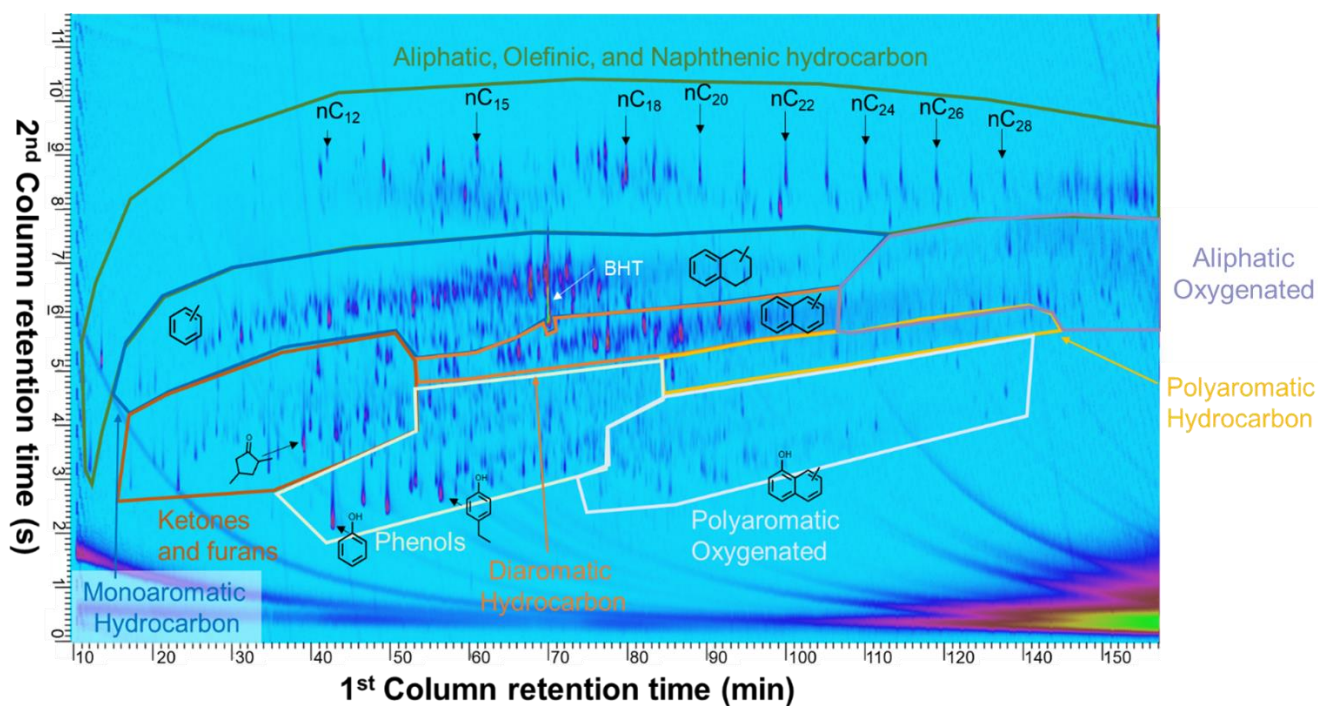
250 The functional group's composition, determined by ¹³C NMR, of the crude oil is shown in Table 3. The
251 crude oil is mainly composed of aliphatic (53.6%) and aromatic (40.3%) carbon. Among the aromatic
252 carbon, 24.0% corresponded to C-H bonds, 9.6% to C-C bonds, and 6.8% to C-O bonds (chemical shift
253 and NMR Spectrum in Table S2 and Figure S2, respectively). Alkyl groups or polyaromatics compounds
254 in crude oil can explain the occurrence of C-C bonds in aromatic fraction. Additionally, the high
255 incidence of aromatic C-O and carbonyl C=O, compared to the methoxy, aliphatic, carboxylic acid, and
256 esters, indicates that phenolic compounds and ketones represent a significant portion of the crude oil
257 oxygen. Indeed, the crude oil composition analysis by comprehensive GC×GC-TOFMS (Figure 1)
258 showed the presence of ketones, furans, phenols, and naphthols. A small amount of mono-aromatic

259 and di-aromatic hydrocarbons and non-aromatic cyclic hydrocarbons, possibly derived from
 260 biomarkers typically present in lignites²⁷, were also found. The quantification performed by GCxGC-
 261 FID is shown in Table 4. Only 16.7 wt.% of the crude oil sample was detectable by GCxGC-FID analysis.
 262 The non-detected compounds were too heavy to be analyzed by gas chromatography. Indeed, Liu et
 263 al. analyzed the heteroatom-containing compounds obtained from the ethanolysis of lignite via
 264 Fourier transform ion cyclotron resonance mass spectroscopy (FTICR-MS), observing a significant
 265 number of oxygenated compounds with up to 6 aromatic rings with the particular occurrence of
 266 oxygenated molecules with carbon number between 17 and 26 carbons and two oxygen atoms, like
 267 organic acids and diols²⁸. In the same study, authors characterized the sulfur-containing compounds,
 268 mostly ranging above C₂₀ and associated in the same molecule with another S or several O atoms.²⁸
 269 The relatively large carbon number of the sulfur-containing compounds in crude oil can explain the
 270 few S compounds detected in the products by comprehensive GCxGC-TOFMS (Figure 1). Indeed, the
 271 analysis of the sulfur content of the crude oil sample by GC-FPD⁺ using a Simdis chromatography
 272 method equivalent to ASTM D2887 reveals that such molecules have a retention time higher than
 273 hexatriacontane (C₃₆ - Bp = 497 °C) (Figure S3), which defines the upper detection limit of the GCxGC
 274 analysis. The same explanation can be given for the few nitrogen-containing compounds among the
 275 GCxGC detected compounds in the crude oil (Figure 1).

276 Table 3. Composition of crude oil obtained from the HTL of Bełchatów lignite

Composition		Carbon chemical composition (¹³ C NMR) ^a	
C (wt.%)	77.7 ± 0.1	C _{Aliphatic}	53.6
H (wt.)	8.9 ± 0.3	C _{Methoxy} (-O-CH ₃)	0.1
O (wt.%)	10.8 ± 1.0	C _{Aliphatic-O} (-O-(CH ₂) _n)	0.8
S (ppm)	2.4 ± 0.1	C _{Aromatic}	40.3
N (ppm)	0.5 ± 0.1	C _{Carboxylic/Amide}	0.8
TAN (mg _{KOH} /g)	29.2 ± 0.2	C _{Aldehyde/Ketone}	4.4
HHV (MJ/kg)	31.8		

277 ^aChemical shift range in Table S1 and NMR spectra in Figure S2



278

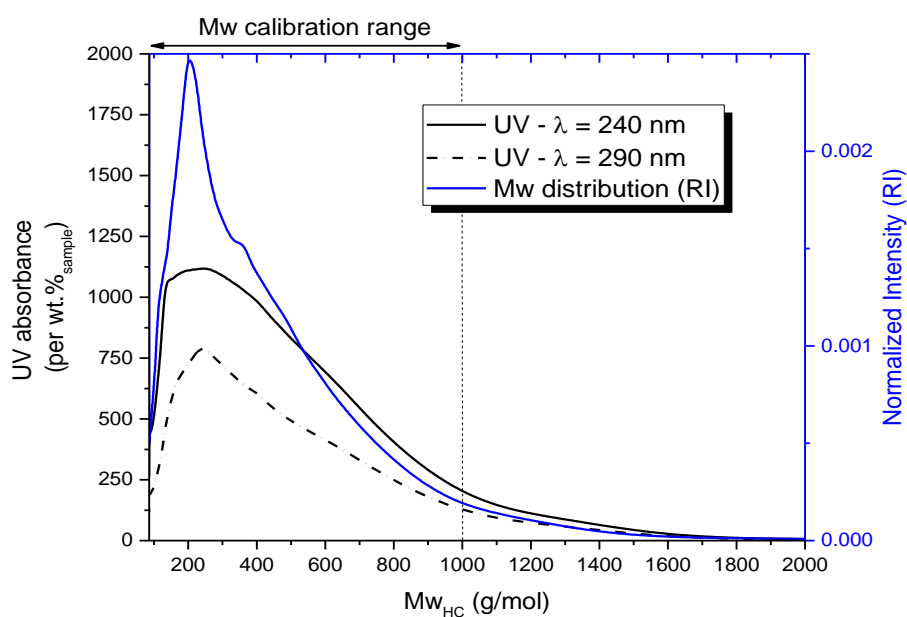
279 Figure 1. GCxGC-TOF MS chromatogram of the crude oil obtained from the HTL of lignite. BHT
 280 (butylated hydroxytoluene) originates from THF solvent, where it serves as a stabilizer.

281

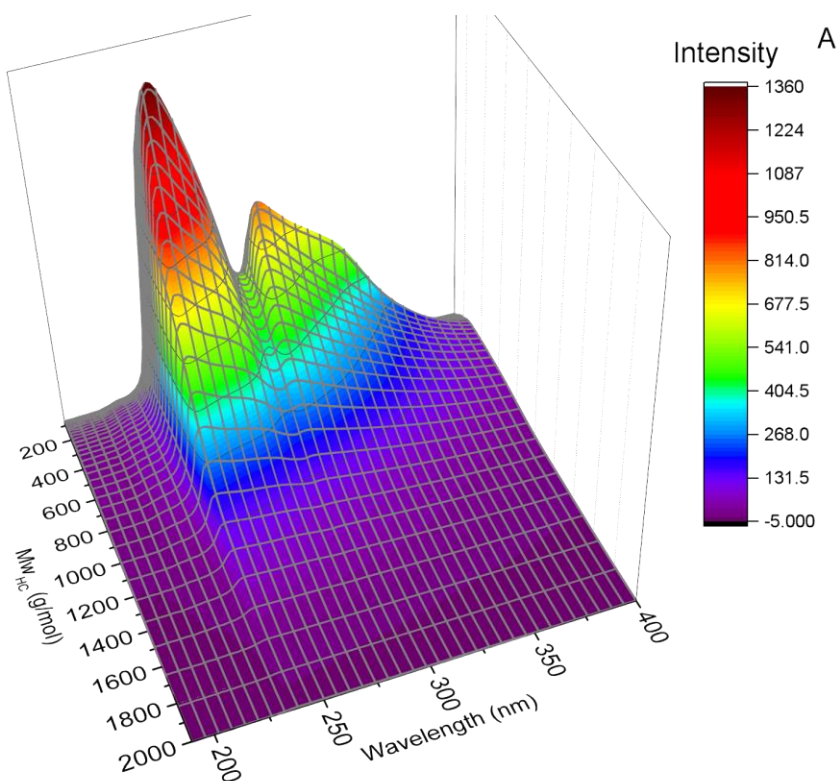
282 Table 4. Quantification of the lignite HTL oil compounds detected by GCxGC-FID using the relative
 283 response factor method (supporting information). The chromatogram and the areas attributed to
 284 each compound family are represented in Figure 1.

Compounds	Oil composition (wt.%)	Compounds	Oil composition (wt.%)
Aliphatic HC	1.6	Ketones and furans	0.6
Monoaromatic HC	1.6	Phenols	1.4
Diaromatic HC	1.6	Polyaromatic Oxygenated	2.2
Polyaromatic HC	1.2	Aliphatic Oxygenated	6.5

285



286



287

288 **Figure 2.** A) Compounds in the liquid product molecular weight (Mw_{HC}) distribution determined by
 289 refraction index (RI) (blue curve) and UV absorbance ($\lambda = 240$ nm and 290 nm) as a function of the
 290 compounds Mw. Average Mw = 297 g/mol. B) DAD spectrum ($\lambda = 190 - 400$ nm) of crude oil as a
 291 function of molecular weight (Mw_{HC}).

292

293 A better insight into heavy molecules is given by SEC. The molecular weight distribution of the crude
294 oil components (Figure 2-A) reveals a large range of compounds, with a molecular weight of up to
295 ~1,800 g/mol in HC eq. and an average molecular weight of 297 g/mol in HC eq. The significant
296 presence of large Mw molecules, which are expected to have a high boiling point, agrees with the
297 small detection level observed in the GCxGC analysis. The evolution of the DAD spectra as a function
298 of molecular weight (Figure 2-B) reveals an intense absorption between 240 and 400 nm, reflecting
299 the high aromatic nature of the compounds in the crude oil. The presence of two absorption
300 maximums, 245 nm and 293, and a shoulder at 316 nm indicates that polyaromatic compounds are
301 abundant in the crude oil sample. Indeed, as exemplified in Figure S4, monoaromatic compounds like
302 benzene generate a DAD band at ~250 nm. In opposition, polyaromatic compounds with two or more
303 conjugated aromatic rings present a second absorption band at $\lambda > 290$ nm (Figures S5, S6, and S7). In
304 the particular case of naphthalene, a second sharp peak was observed at 290 nm, with identical
305 intensity to the peak centered at 250 nm (Figure S5), while in anthracene and pyrene, this band is
306 significantly broader, extending to significantly higher λ (Figures S6 and S7). Therefore, in the crude
307 oil (Figure 2-A), the wide absorption band at $250 > \lambda > 400$ nm indicates the presence of compounds
308 with at least 3 and 4 conjugated aromatic rings.

309 The comparison of the Mw distribution and the UV absorbance at $\lambda=240$ nm and 290 nm as a function
310 of the Mw reveals that both RI and UV curves have a maximum at Mw ~ 230 g/mol (Figure 2-A).
311 However, the UV spectra absorption distribution is shifted to higher Mw, evidencing heavier
312 molecules with high aromaticity.

313

314 **3.1.2. Char, gas, and aqueous phase**

315 The hydrothermal liquefaction of lignite (soft Miocene lignite) obtained in the Bełchatów coal mine in
316 Poland led to four product streams, i.e., gas, char, crude oil, and an aqueous phase rich in organic
317 matter. Char was the most abundant among the product streams, representing 48.8 wt.% of the lignite

318 feedstock yield. Even though char and lignite are both solids, the former displayed a higher carbon
319 content with lower oxygen, nitrogen, hydrogen, and sulfur (Table S4). Hence, char displayed O/C and
320 H/C ratios of 0.1 and 0.4, respectively, while lignite O/C was 0.2 and H/C was 1.1. The different solid
321 composition explains char's slightly higher heating value compared with the lignite feedstock, i.e., 22.6
322 MJ/kg_{Dry} vs. 19.0 MJ/kg_{Dry}, respectively. P. Liu and D. Zhang²⁹ studied the transformation of lignite
323 under hydrothermal conditions, observing that, at T=260 °C, significant removals of oxygen and
324 hydrogen occur. Similar observations were made by Z. Shi et al.³⁰, who, like P. Liu and D. Zhang,
325 observed a significant reduction of carboxyl, carbonyl, and oxygenated aliphatic carbon in the solid
326 after HTL treatment. These authors also observed a reduction of the aliphatic CH₂ and CH₃ groups after
327 hydrothermal treatment, which justifies the decrease in the H/C ratio. The authors linked the
328 elimination of oxygen and hydrogen from the lignite structure to the production of light gases, such
329 as CO, CO₂, and light hydrocarbons^{29,30}. Like O and H, the sulfur in char was significantly smaller than
330 in the lignite feedstock, i.e., 1.1 wt.% vs. 3.78 wt.%, respectively, indicating only 14.2 % of sulfur
331 remained in the solid phase after hydrothermal liquefaction. The significant extent of desulfurization
332 is directly related to the nature of the sulfur compounds in lignite. As low-ranking coals, lignites
333 contain more substantial amounts of sulfides and thiols than other types of coal³¹, which are more
334 easily transformed under hydrothermal conditions^{32,33}.

335 The lower impurities content, i.e., O, N, and S, and increased calorific value indicate that char is a
336 higher quality coal than the original lignite. Indeed, the treatment of coal samples through
337 hydrothermal liquefaction has been demonstrated to increase the quality of coal samples, both by
338 eliminating impurities and improving hydrophobicity^{12,30,34,35}.

339 The composition of the gas stream formed during the hydrothermal liquefaction of lignite is shown in
340 Table S5. CO₂ was the majority product in the gas phase, corresponding to 92.6 wt.% of all the
341 produced gases. The high CO₂ selectivity in the gas products obtained from lignite HTL had already
342 been reported previously^{15,30}, indicating that decarboxylation is one of the primary processes
343 responsible for oxygen removal during the reaction. Indeed, CO only represented 1.4 wt.% of the

344 gases, suggesting decarbonylation is significantly less favored. H₂S represents the second most
345 abundant compound in the gas stream, representing 3.4 wt.% of all gases. Furthermore, 19.4% of the
346 sulfur in the lignite feedstock was transformed into H₂S. The significant formation of H₂S reflects the
347 transformation of organic, i.e., thiol and sulfide, and inorganic sulfur, i.e., pyrite, compounds in lignite
348 promoted by H radicals under hydrothermal conditions^{32,33,36}. In addition to CO₂, CO, and H₂S, small
349 amounts of light hydrocarbons and H₂ (Table S5) were also observed. Nonetheless, the amount of such
350 compounds is not enough to justify alone the small H/C observed in the char, thus suggesting that
351 light hydrocarbons and H₂ formation are not the main ones responsible for the elimination of
352 hydrogen in the lignite as proposed by Z. Shi et al., and P. Liu and D. Zhang^{29,30}. Instead, the
353 transformation of lighter fractions of lignite into aqueous and crude organic compounds is more likely
354 to cause the low H/C of char compared to lignite.

355 Finally, the organic matter solubilized in the aqueous reaction media, i.e., the aqueous phase,
356 represented 15.9 wt.% of feedstock lignite. In hydrothermal liquefaction processes, the aqueous
357 phase is typically composed of organic acids, e.g., acetic acid, oxygenated aromatics, aromatic, like
358 phenols, nitrogenated compounds, and oxidized sulfur compounds^{33,37,38}, thus justifying this stream's
359 acidic pH of 5.2.

360

361 **3.2. Hydrotreatment of lignite HTL crude oil**

362 The significant concentration of heteroatoms and polyaromatic compounds in the crude oil stream
363 clearly demonstrates the necessity of further upgrading for the production of hydrocarbon fuels.
364 Therefore, this section will focus on the hydrotreatment of the crude oil stream obtained from the
365 hydrothermal liquefaction of lignite. The hydrotreatment of the lignite crude oil was performed at
366 three different temperatures, i.e., 350 °C, 375 °C, and 390°C, and at two different reaction times, 1 h
367 and 3 h. An additional residence time, where the reaction was stopped after the reaction temperature
368 was attained ($t_{\text{heating}} = 20 \text{ min}$), designated $t = 0 \text{ h}$, was also performed at each temperature. The crude

369 oil conversion occurring before $t = 0$ h are caused primarily by thermal processes. For each operating
370 condition, five product streams (Figure 3-A) were obtained, i.e., gas, liquid, solid, and H_2S and H_2O
371 estimated using equations 9 and 10.

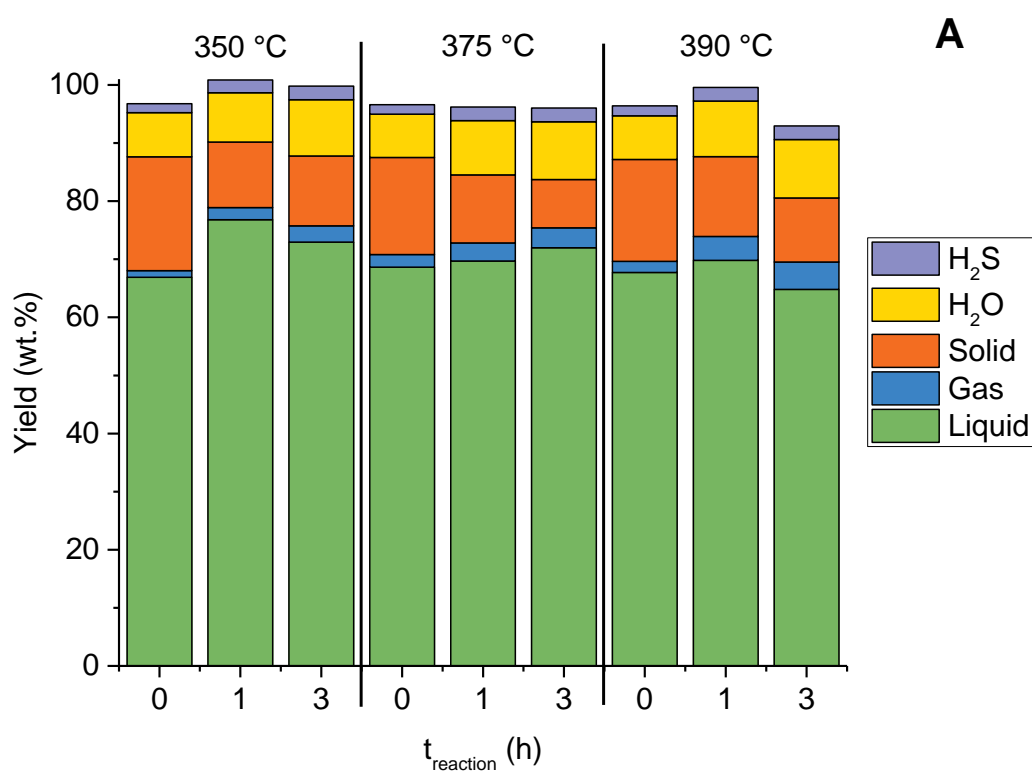
372 **3.2.1. Solid product**

373 The solid product was found to decrease as a function of the reaction time. Indeed, for the $t = 0$ h
374 experiments, the solid fraction yield was $\approx 16.7 - 19.6$ wt.%, while the solid yield decreased to $\approx 9 - 12$
375 wt.% for longer residence time. It should be mentioned that no solid products, such as char, other
376 than the spent catalyst, could be visually observed after the reaction. Consequently, at least part of
377 the solid product is represented by heavy asphaltene-like products that can be converted under the
378 reaction conditions but are not soluble in heptane and stay with the catalyst after the reaction. Table
379 S6 contains the carbon loading of the spent catalyst after the reaction, showing that higher reaction
380 time and temperatures lead to lower carbon deposition on the catalyst's surface. Furthermore, at the
381 temperature of $375^\circ C$ and $390^\circ C$ after 3 h, the carbon deposition on the spent catalyst was ≈ 5 wt.%,
382 which is compatible with the typical coke loadings observed in the early stages of operating HDT
383 catalysts³⁹. Hence, the crude oil feedstock did not lead to enhanced deactivation by coke deposition
384 of the sulfided catalyst, as observed for HTL crude oils from other sources, like sewage sludge⁴⁰.

385 **3.2.2. Gas product**

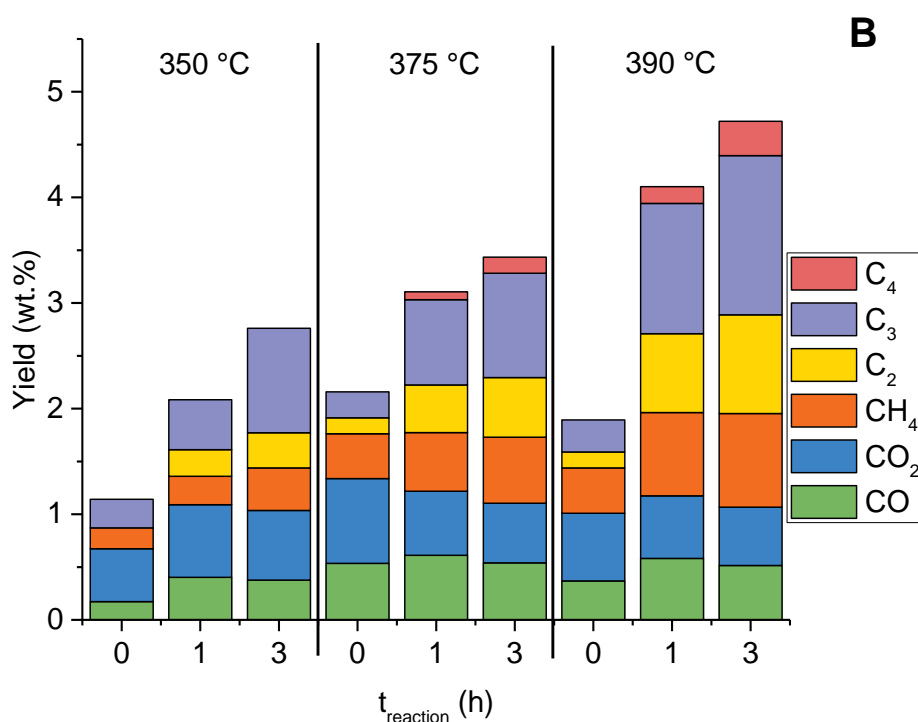
386 The yield and composition of the gas products are shown in Figure 3-B. In general, the yield of gas
387 increases with the reaction temperature and reaction time, achieving a maximum of 4.7 wt.% for the
388 reaction conditions of $390^\circ C$ and 3 h. Still, the yield of gas products like CO and CO_2 , which result from
389 decarboxylation and decarbonylation reactions, was found to stay constant, between 0.4-0.6 wt.%
390 and 0.6 – 0.8 wt.%, respectively, after 1 h of reaction independently of the temperature (Figure 3-B).
391 The low yield of CO and CO_2 is attributed to the minor contribution of aliphatic C-O, methoxy, and acid
392 groups in the crude oil (Table 3). Indeed, the oxygen in the crude oil was primarily eliminated as H_2O ,
393 whose yield is between 7.5 wt.% and 10.0 wt.%. Light hydrocarbons, like CH_4 , C_2H_6 (C_2), C_3H_8 (C_3), and

394 C₄H₁₀ (C₄), were the main compounds responsible for the gas yield increase observed at higher
 395 temperature and reaction time (Figure 3-B). While the formation of light hydrocarbons can be
 396 explained by C-C bond cleavage caused by hydrogenolysis, which is favored at higher temperatures,
 397 heptane cracking does not seem to contribute significantly to the gas products since the $\frac{C_3}{C_4}$ ratio is
 398 significantly higher than 1 (Figure 3-B). Indeed, on sulfided catalysts, like NiMoS/P-Al₂O₃, heptane
 399 hydroconversion occurs preferably through β -scission, yet this mechanism only becomes relevant at
 400 temperatures above the ones used in this study, i.e., T > 400 °C^{41,42}. Instead, light hydrocarbons most
 401 likely result from the cleavage of larger molecules from the crude oil during the hydrotreatment
 402 reaction.



403

404



405

406 Figure 3. A) Product yields, determined according to equations 6 to 10, obtained from the HDT of the
 407 lignite HTL crude oil. B) Gas products yield as a function of reaction temperature and time, obtained
 408 from the HDT of the lignite HTL crude oil.

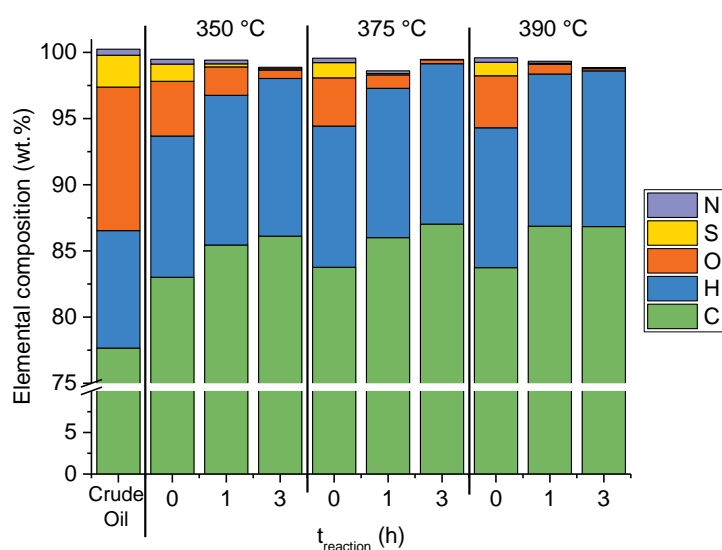
409

410 **3.2.3. Liquid product**

411 After upgrading, the liquid product yield varied between 65 wt.% and 77 wt.% depending on the
 412 reaction temperature and time (Figure 3-A). In all cases, the liquid yield was slightly higher after 1 h of
 413 reaction as compared to $t_{\text{reaction}} = 0$ h, which agrees with the hypothesis previously stated on the
 414 conversion of solid products existing at the early stages of the reaction (section 3.2.1). After 3h of
 415 reaction, the liquid produced stabilized at 375 °C or slightly decreased at 350 °C and 390 °C due to the
 416 lower amount of solid converted in this time (Figure 3-A and Table S6) and the HDT reactions.

417 The elemental composition of the HDT liquid product is shown in Figure 4. When compared with the
 418 crude oil feedstock (Table 3), the HDT liquid products contained a higher concentration of carbon and
 419 hydrogen (Figure 4) even at $t_{\text{reaction}} = 0$ h. Similarly, the concentration of heteroatoms in the liquid
 420 product was also significantly smaller at $t_{\text{reaction}} = 0$ h than on the parent crude oil sample, with

421 deoxygenation, denitrogenation, and desulfurization in the range of 60%, 30% and 50% respectively
 422 (Tables S7 to S9). It should be mentioned during heating, H₂ pressure is reduced (10 bar, at room
 423 temperature) and that heating up to the reaction temperature takes 20 min. Thus, the significant
 424 elimination of heteroatoms during heating suggests these be easily removable under relatively mild
 425 conditions or by thermal degradation. Furthermore, HDO, HDS, and, to a lesser extent, HDN (Tables
 426 S7 to S9) significantly increased with the reaction time, reaching above 94 %, 96 %, and 78%,
 427 respectively, after 3 h of reaction. On the other hand, high denitrogenation levels required a higher
 428 temperature, such as 390 °C, with the HDN rate being significantly favored at higher temperatures.
 429 The efficient removal of heteroatoms suggests that the hetero-compounds in the crude oil feedstock
 430 are not in the form of refractory compounds, i.e., polyaromatic sulfur and nitrogen compounds^{43,44}, as
 431 indicated by Liu et al.²⁸. It is relevant to mention that most HTL crude oils from bio-sourced feedstocks,
 432 like algae, food waste, and sewage sludge, require two stages of upgrading to remove heteroatoms
 433 effectively^{37,45,46}. Yet, nearly all lignite crude oil's sulfur, nitrogen, and oxygen were removed after a
 434 single hydrotreatment step on NiMoS/P-Al₂O₃ catalyst. Still, in the best-case scenario, 30 ppm of sulfur
 435 was found in the liquid, indicating further desulfurization via a second HDT stage, harsher conditions,
 436 or blending is necessary to meet the minimum requirements of a drop-in fuel from lignite crude oil.



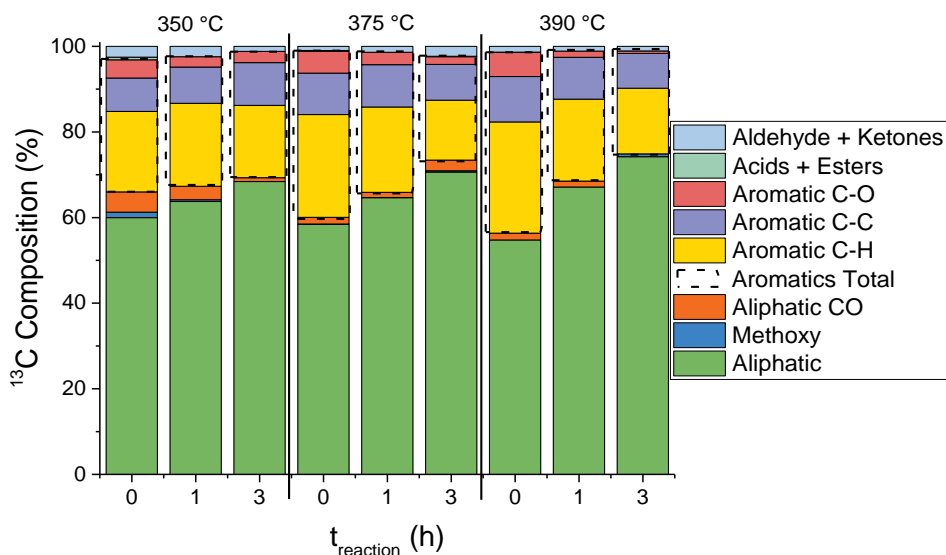
437

438 Figure 4. Elemental analysis of lignite crude oil and the liquid product obtained from HDT of lignite
439 crude oil at different reaction temperatures (350 °C, 375 °C, and 390 °C) and reaction times (t_{reaction}).

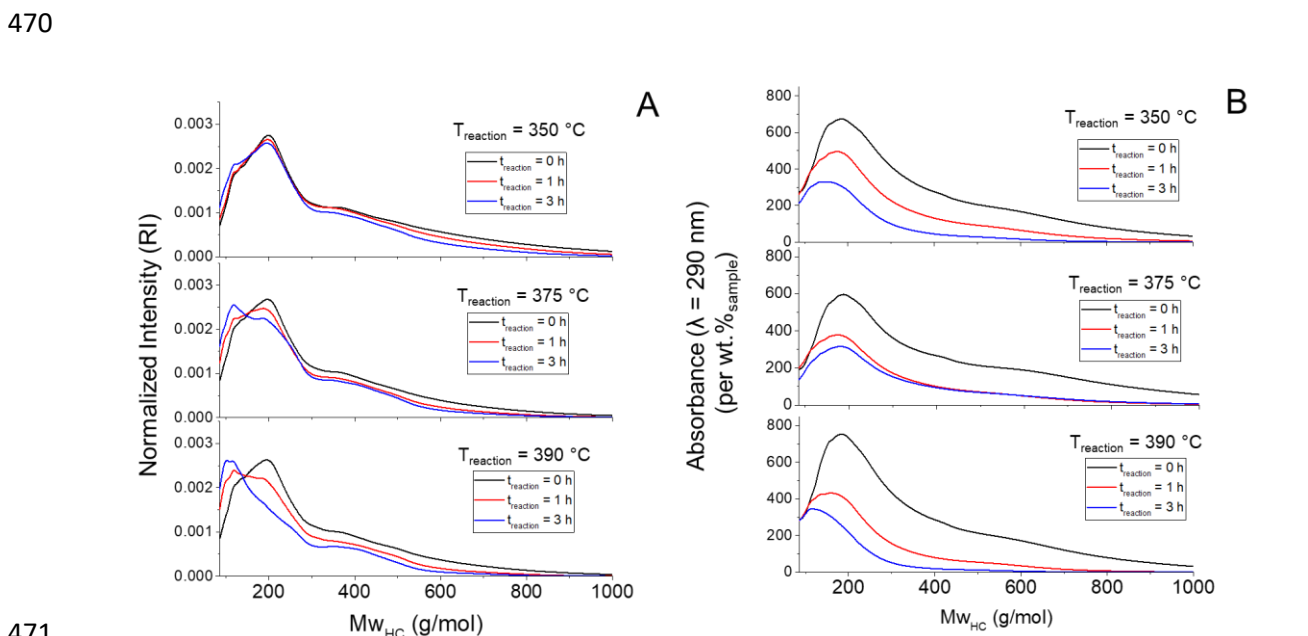
440

441 The evolution of the functional groups upon HDT, determined by ^{13}C NMR, is shown in Figure 5. In
442 comparison with the crude oil, the distribution of the functional groups of the liquid product clearly
443 shows a significant increase in the aliphatic carbon, i.e., from 40.1%, in crude oil, to 54.8 – 74.2% in
444 the liquid, accompanied by a reduction of the aromatic carbon, i.e., 54.3% to 42.3 – 24.0%. When
445 comparing the HDT liquids composition obtained at $t_{\text{reaction}} = 0$ h, it can be observed that the
446 concentration of aromatic C-H and C-C increases with temperature. In contrast, the occurrence of
447 functional groups containing oxygen and aliphatic C follows the opposite trend (Figure 5). At $t_{\text{reaction}} =$
448 0 h, the aromatic carbon concentration was observed to increase with the reaction temperature,
449 suggesting that thermal condensation occurs during reactor heating. Indeed, the UV absorption at
450 $\lambda=290$ nm (Figure 6-B), characteristic of polyaromatic compounds, which can be formed by unstable
451 products in the crude oil during heating, clearly increases as a function of temperature for $T = 0$ h. As
452 the reaction time increases, the concentration of aliphatic C increases together with a reduction of
453 aromatic C as a consequence of hydrogenation, as confirmed by the H/C ratio increase from ≈ 1.5 at 0
454 h to >1.6 after 3 h for reaction (Figure 4). Additionally, the $\frac{C_{\text{Aliphatic}}}{C_{\text{Aromatic}}}$ ratio increases more with the
455 reaction time for higher temperatures due to the faster kinetics of the HDT reactions promoted by the
456 catalyst. While HDT significantly reduced the concentration of aromatic C-H bonds, the concentration
457 of aromatic C-C only decreased slightly at 375 °C and 390°C and even increased at 350 °C (Figure 5).
458 Additionally, the $\frac{C-C_{\text{Aromatic}}}{C_{\text{Aromatic}}} \cdot 6$ (where 6 refers to the number of carbon atoms in one aromatic ring),
459 which accounts for the average number of C-C_{Aromatic} bonds per aromatic ring, increased from 1.5 at 0
460 h to 2.0 after 3 h of reaction. It should be mentioned that aromatic C-C bounds can result from
461 polyaromatic hydrocarbons, partially hydrogenated polycyclic-aromatics, like tetraline, and alkylated
462 aromatics, such as toluene. Aromatic ring hydrogenation in polyaromatic compounds decreases for
463 each ring already hydrogenated in the molecule^{43,47,48}. Indeed, our previous work screening the

464 upgrading of various HTL oils has already demonstrated that lignite crude oils were particularly rich in
 465 aromatic compounds, which results in a significant concentration of naphthenes and cyclic
 466 monoaromatic compounds after HDT⁴⁹.



467
 468 Figure 5. ¹³C functional group composition of the liquid product obtained from HDT of lignite crude oil
 469 at different reaction temperatures (350 °C, 375 °C, and 390 °C) and reaction times (t_{reaction}).



471
 472 **Figure 6.** A) Liquid product molecular weight (Mw_{HC}) distribution determined by refraction index (RI),
 473 and B) UV absorbance ($\lambda = 290 \text{ nm}$) as a function of the compounds Mw. A hydrocarbon mixture with
 474 Mw comprised between 86 g/mol and 1000 g/mol was used as a standard to determine Mw_{HC} .

475

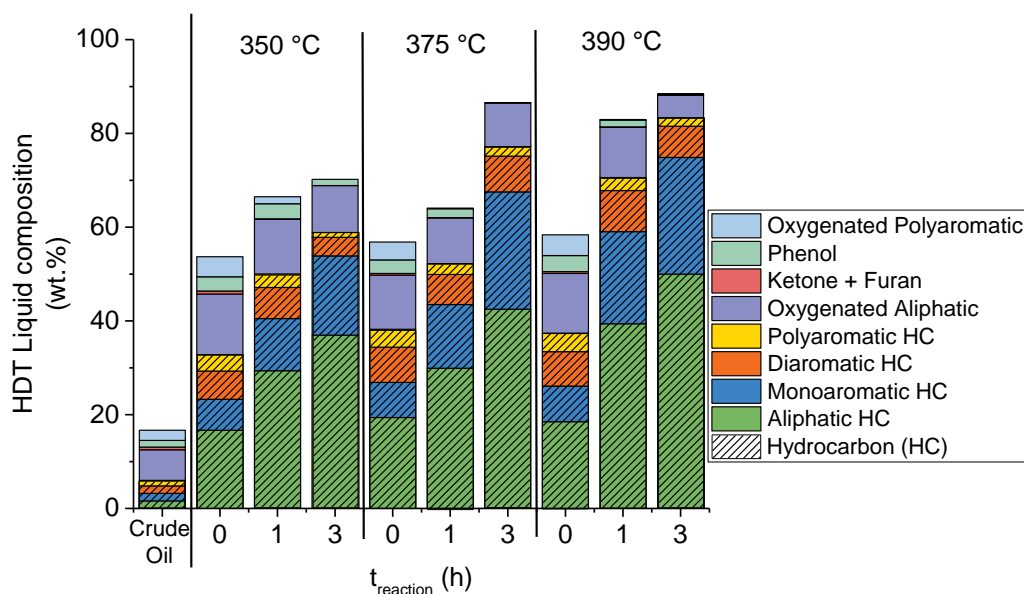
476 The molecular weight ($M_{w_{HC}}$) distribution of the HDT liquid products is shown in Figure 6A. At low
477 reaction time, the $M_{w_{HC}}$ distribution presented a maximum centered at ≈ 200 g/mol and a maximum
478 molecular weight of 1 000 g/mol. As the reaction time increased, the compounds centered at 200
479 g/mol progressively decreased as a new group of compounds centered at ≈ 120 g/mol appeared.
480 Similarly, the higher molecular weight compounds progressively disappeared, and at 390 °C after 3 h
481 of reaction, no compounds above 800 g/mol were detected. Indeed, the degree of $M_{w_{HC}}$ reduction
482 observed in the liquid products after HDT highly depended on the reaction time and temperature,
483 with the average $M_{w_{HC}}$ (Table S10) ranging from 243 g/mol to 160 g/mol. The average molecular
484 weight of the liquid products is reported in Table S10.

485 The removal of the heteroatom elements, i.e., O, N, and S, is considered to be the main responsible
486 for the significant $M_{w_{HC}}$ reduction since the cleavage of C-C bonds via hydrogenolysis is not
487 predominant under the reaction conditions used in this study.

488 Figure 6B shows the absorbance at $\lambda=290$ nm, characteristic of conjugated polyaromatic compounds,
489 as a function $M_{w_{HC}}$. The absorbance decreases as a function of the reaction time due to the full or
490 partial hydrogenation of the polyaromatic compounds. Still, Figure 6B clearly shows that
491 polyaromatics undergo faster conversion in the first hour of a reaction than in the subsequent 2 h.
492 Also, at all temperatures, the UV absorption for $M_{w_{HC}} > 300$ g/mol decreases fast during HDT, with
493 nearly all polyaromatics in this range being converted at $T = 390$ °C after 3 h of reaction. However, the
494 refraction index detector (RID – Figure 6A) clearly shows that the amount of compounds with a $M_{w_{HC}}$
495 > 300 g/mol are only reduced slightly during HDT. The difference between the two detectors suggests
496 that higher $M_{w_{HC}}$ polyaromatic compounds undergo hydrogenation faster. Indeed, Korre et al. studied
497 the hydrogenation kinetic of multiple polyaromatic compounds identifying that the higher the number
498 of conjugated rings, the faster the hydrogenation reaction rate⁵⁰.

499 The composition of the liquid product, quantified by comprehensive GC×GC/FID (Figure 7), shows a
500 progressive increase in the concentration of aliphatic and mono-aromatic hydrocarbon under harsher
501 reaction conditions, as already suggested by ¹³C NMR (Figure 5), SEC-DAD (Figure 6B), and elemental
502 analysis (Figure 4) results. At the same time, the oxygenated compounds, such as phenols, ketones,
503 furans, and other high molecular weight compounds, are progressively transformed. Furthermore, the
504 concentration of compounds in the comprehensive GC×GC-FID analysis detection range, i.e., up to
505 ≈C₄₀, progressively increased with HDT reaction time and temperature, which is a consequence of the
506 reduction of the Mw of the samples (Figure 6A). At 390 °C and 3 h of reaction, 88.4 wt.% of the HDT
507 liquid product composition was quantified, with aliphatic and monoaromatic hydrocarbon, mainly
508 composed of naphthenes and partially hydrogenated aromatics, respectively, contributing to ≈75%
509 of the sample. Additionally, 9 wt.% of the liquid was composed of polyaromatic hydrocarbons with
510 two or more aromatic rings. The high concentration of cyclic hydrocarbons in the liquid is a direct
511 consequence of the aromatic nature of the products in the crude oil and, by extension, in lignite.
512 Indeed, in our previous work, we demonstrated that the nature of the feedstock was crucial in
513 determining the composition of the HDT liquid product and that lignite led to an HDT liquid rich in
514 cyclic hydrocarbons⁴⁹.

515 As mentioned before, lignite crude oil was already transformed during the 20 min heating stage of the
516 reactor, as easily observable by the comprehensive GC×GC's significant compound detection boost,
517 i.e., 16.7 wt.% to >56.7 wt.%. While the increase in aromatic content in the liquid showed that thermal
518 phenomena caused at least part of the transformation, the rise in detectable aliphatic and
519 monoaromatic hydrocarbon compounds suggests that catalytic HDT was also responsible for the
520 transformation of the feedstock during the heating stage, indicating that lignite crude oil can undergo
521 significant heteroatoms removal, even under relatively mild conditions.



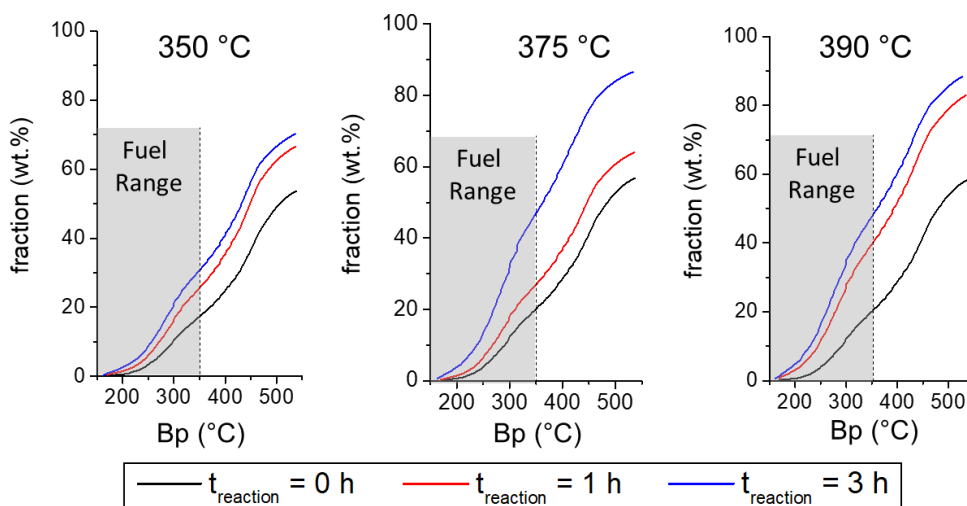
522

523 Figure 7. Composition of lignite crude oil and the HDT liquid as a function of the reaction temperature
 524 (350 °C, 375 °C, and 390 °C) and reaction time (t_{reaction}) detected by GCxGC-TOFMS (Figure S8) and
 525 quantified by GCxGC-FID.

526

527 The distillation curves for the HDT liquid products are shown in Figure 8. As expected from the
 528 reduction of Mw distribution observed in the SEC results (Figure 6A), the number of products in the
 529 fuel range increases with the reaction temperature and time. While at 0h, the fuel range products
 530 concentration is quite similar at all temperatures (17-20 wt.%), fuel yield quickly rises with the reaction
 531 time (Table S11). It is worth mentioning that oxygenated products, like phenols, are present in the fuel
 532 range products (boiling point < 350 °C) in all cases, except for the experiments performed at 375°C
 533 and 390 °C after 3 h of reaction, which are exclusively composed of hydrocarbon molecules.
 534 Additionally, diaromatic hydrocarbons are present in all cases and makeup \approx 5 wt.% of the fuel range
 535 products obtained at 375°C and 390 °C after 3 h of reaction. Additionally, the maximum fuel yield
 536 obtained at 375°C and 390°C was 47.0 wt.% and 47.6 wt.%, respectively, showing that increasing the
 537 HDT temperature has little effect on the overall fuel yield after the elimination of most heteroatoms
 538 (Figure 4). Still, a slight variation in the composition of the fuel range products was observed (Tables

539 S12 and S13), with the test at 375°C yielding more products, i.e., 33.5 wt.% Vs 30.8 wt.%, in the middle
 540 distillates range (Bp between 250°C and 350°C) and the test at 390°C being more selective for
 541 kerosene (Bp between 175°C and 250 °C), i.e., 14.7 wt.% Vs. 11.9 wt.%. The increase in lower Bp
 542 products observed at 390 °C might be associated with C-C hydrogenolysis, favored by a higher
 543 temperature.



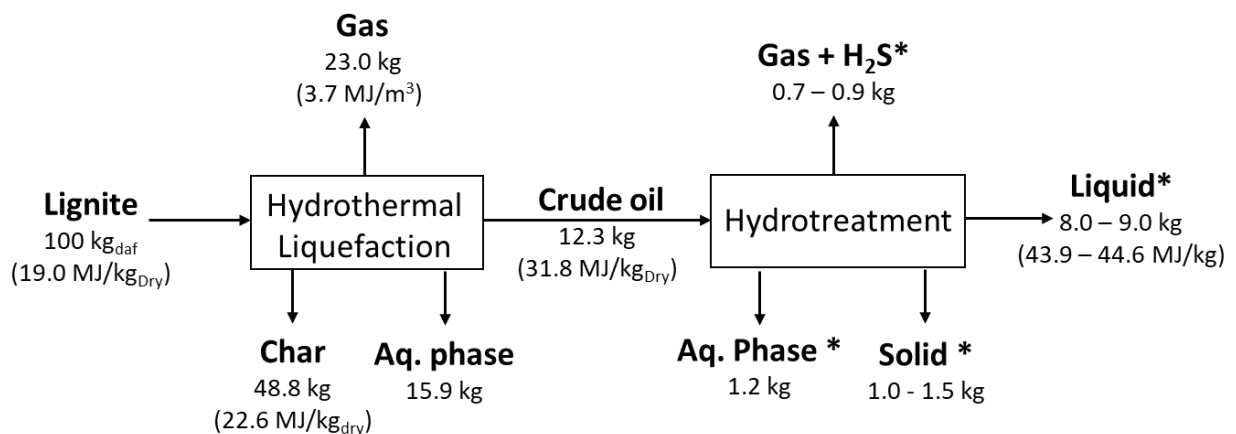
544
 545 Figure 8. Distillation curve of the hydrotreatment liquid product as a function of reaction time (t_{reaction}).
 546 Fuel range: Bp < 350°C.

547
 548 The overall mass balance of the process, shown in Figure 9, indicates that the HDT liquid yield obtained
 549 from lignite under the HTL and HDT conditions used in this study is 8-9 wt.% and 47 wt.% of HDT liquid
 550 products have a boiling point in the range of standard fuels, i.e., Bp < 350°C (Figure 8). The low yield
 551 of crude oil during HTL, i.e., 12.3%, is responsible for the low overall conversion of lignite into fuel.
 552 Indeed, the HDT liquid yield obtained in this study, i.e., 65-73 wt.%, was comparable to that in the
 553 literature when upgrading HTL biocrudes produced from different feedstocks⁵¹⁻⁵⁵. The low crude oil
 554 yield can be explained by the experimental conditions used in the HTL process, as Liu et al. were able
 555 to increase the crude oil production to 34 wt.% by using a lower HTL reaction time (5 min) and higher
 556 temperature (440 °C). Additionally, the use of catalysts⁵⁶ and recycling the aqueous phase⁵⁷ are known

557 to increase crude yield during HTL. Therefore, adequate process optimization can orient a more
 558 significant fraction of lignite towards fuel generation.

559 While lignite is not a green feedstock, its easily upgradable products obtained during HTL can be
 560 beneficial under mixed hydrothermal liquefaction with greener feedstocks, like lignocellulosic
 561 biomass, sewage sludge or algae, which yield crude oils more difficult to upgrade as proposed, for
 562 instance, by Wang et al.⁵⁸. Indeed, it was shown that the hydrothermal liquefaction of a mixture of
 563 Jingou lignite, wheat straw, and plastic waste could provide a synergetic effect on oil yields. Synergetic
 564 effects were also observed in the co-liquefaction of coal and polymers (polypropylene and
 565 polystyrene) by Y. Shen et al.⁵⁹. Finally, it is worth mentioning that the char from lignite HTL can be
 566 further used for electricity production, the original purpose of lignite.

567



568

569 Figure 9. Block flow diagram of the transformation of lignite through hydrothermal liquefaction (HTL)
 570 and subsequent hydrotreatment of the HTL crude oil. Mass basis = 100 kg of dry ash-free lignite (kg_{daf}).
 571 The values in brackets refer to the calorific value of the respective streams and were determined by
 572 using the expression from⁶⁰. *values determined using the data from HDT performed during 3 h at
 573 temperatures of 375°C and 390°C (Figures 3-A and 4).

574

575

576

577 4. CONCLUSION

578 In several European countries, gross electricity is partly generated by the combustion of lignite. Here,
579 we propose diverting one fraction of the lignite to produce kerosene and diesel through an HTL and
580 single-stage HDT sequence. After HTL, only 12.3% of lignite was converted into crude oil. The low yield
581 was attributed to the low temperature ($T = 360\text{ °C}$) and high contact time ($t_{\text{contact}} = 30\text{ min}$) used. The
582 crude oil obtained from HTL was mainly composed of high molecular weight compounds, up to 2,000
583 g/mol, which were particularly rich in oxygen (10.8 wt.%) and sulfur (2.4 wt.%). In addition to the crude
584 oil, the lignite HTL also produced a char stream (48.8 wt.%) with the potential to be valorized for
585 electricity production, the original purpose of lignite.

586 The hydrotreating experiments showed lignite's crude oil to be quite easily hydrotreated. Near
587 complete S and O removal was achieved with a single HDT stage and using a milder pseudo-WHSV
588 (equation 5) than those reported in the literature for pilot-scale bio-based crude oil HDT^{53,61}. After
589 HDT, despite a significant improvement in fuel quality, i.e., heteroatom removal and hydrogenation,
590 substantial amounts of aromatic compounds, particularly monoaromatic and diaromatic compounds
591 ($\approx 45\%$ of fuel range products), are still present in all products. This suggests that further upgrading or
592 harsher conditions, i.e., higher contact time and H_2 pressure, are required. Indeed, aromatics have low
593 cetane numbers, which can be detrimental for using the middle distillate in diesel fuels⁶². In addition
594 to decreasing the aromatic content in the liquid product, our results showed that harshening HDT
595 conditions did not significantly increase the fuel range products, suggesting that subsequent
596 hydrocracking or using an HDT catalyst with acid properties might be necessary. Nevertheless, the
597 crude oil obtained from the hydrothermal liquefaction of lignite has an excellent potential for
598 producing hydrocarbon fuels, particularly when compared with other feedstocks typically used in the
599 HTL process, like sewage sludge and algae^{46,63}. Finally, it is important to mention that the presence of
600 this aromatic fraction can be a benefit, acting as a polar solvent in the case of co-processing between
601 HTL of lignite and less proper biogenic feedstocks, such as biomass or sewage sludge.

602 5. Supporting information

603 HTL experimental and product separation diagram; Catalyst composition; ¹³C chemical shift
604 attribution; GC×GC equipment configuration; HTL char composition; HTL gas yield; Crude oil ¹³C NMR
605 spectrum; crude oil GC/FPD⁺ chromatogram; SEC/DAD of aromatic standards; spent catalyst carbon
606 content; HDT deoxygenation, denitrogenation, and desulfurization results; HDT total fuel, kerosene,
607 and middle distillates yield; GC×GC-TOFMS chromatographs.

608

609 6. Acknowledgements

610 The authors gratefully acknowledge the financial support of the European Commission Research
611 Programme of the Research Fund for Coal and Steel for the project HyCon (Grant agreement: 899471).
612 In the case of Polish authors, this scientific work is published as part of an international project co-
613 financed by the program of the Ministry of Science and Higher Education entitled "PMW" in the years
614 2020 -2023 agreement No. 5157/FBWiS/2020/2021/2

615

616

617

618 7. References

619

- 620 (1) Tollefson, J. What the War in Ukraine Means for Energy, Climate and Food. *Nature* **2022**, No.
621 604, 232–233.
- 622 (2) IEA. *Renewables 2021: Analysis and Forecast to 2026*; Paris, 2021.
623 <https://www.iea.org/reports/renewables-2021>.
- 624 (3) *Renewables 2019*; IEA: Paris, 2019. <https://www.iea.org/reports/renewables-2019>.
- 625 (4) Lignite Energy Council. *Uses and Benefits of Lignite*. [https://lignite.com/what-is-lignite/uses-](https://lignite.com/what-is-lignite/uses-and-benefits-of-lignite/)
626 [and-benefits-of-lignite/](https://lignite.com/what-is-lignite/uses-and-benefits-of-lignite/).
- 627 (5) Eurostat. *Coal production and consumption up in 2022*.
628 <https://ec.europa.eu/eurostat/web/products-eurostat-news/w/ddn-20230622-2>.
- 629 (6) Kershaw, J. R. Extraction of Victorian Brown Coals with Supercritical Water. *Fuel Processing*
630 *Technology* **1986**, 13 (2), 111–124. [https://doi.org/10.1016/0378-3820\(86\)90053-6](https://doi.org/10.1016/0378-3820(86)90053-6).
- 631 (7) Deshpande, G. V.; Holder, G. D.; Bishop, A. A.; Gopal, J.; Wender, I. Extraction of Coal Using
632 Supercritical Water. *Fuel* **1984**, 63 (7), 956–960. [https://doi.org/10.1016/0016-2361\(84\)90318-](https://doi.org/10.1016/0016-2361(84)90318-1)
633 1.
- 634 (8) Hu, H.; Guo, S.; Hedden, K. Extraction of Lignite with Water in Sub- and Supercritical States.
635 *Fuel Processing Technology* **1998**, 53 (3), 269–277. [https://doi.org/10.1016/S0378-](https://doi.org/10.1016/S0378-3820(97)00057-X)
636 [3820\(97\)00057-X](https://doi.org/10.1016/S0378-3820(97)00057-X).
- 637 (9) Nikolopoulos, N.; Violidakis, I.; Karampinis, E.; Agraniotis, M.; Bergins, C.; Grammelis, P.;
638 Kakaras, E. Report on Comparison among Current Industrial Scale Lignite Drying Technologies
639 (A Critical Review of Current Technologies). *Fuel* **2015**, 155, 86–114.
640 <https://doi.org/10.1016/j.fuel.2015.03.065>.
- 641 (10) Hartman, B. E.; Hatcher, P. G. Valuable Crude Oil from Hydrothermal Liquefaction of an
642 Aliphatic Coal. *Energy Fuels* **2014**, 28 (12), 7538–7551. <https://doi.org/10.1021/ef5018708>.

- 643 (11) Liu, P.; Wang, L.; Zhou, Y.; Pan, T.; Lu, X.; Zhang, D. Effect of Hydrothermal Treatment on the
644 Structure and Pyrolysis Product Distribution of Xiaolongtan Lignite. *Fuel* **2016**, *164*, 110–118.
645 <https://doi.org/10.1016/j.fuel.2015.09.092>.
- 646 (12) Li, H.; Wu, S.; Wu, Y.; Wang, H.; Zhang, Z.; Huang, S.; Gao, J. Effects of Hydrothermal Treatment
647 on Physico-Chemical Structures and Liquefaction Behaviors of Lignite. *Fuel* **2020**, *263*, 116636.
648 <https://doi.org/10.1016/j.fuel.2019.116636>.
- 649 (13) Lelevic, A.; Souchon, V.; Geantet, C.; Lorentz, C.; Moreaud, M. Advanced Data Preprocessing
650 for Comprehensive Two-Dimensional Gas Chromatography with Vacuum Ultraviolet
651 Spectroscopy Detection. *Journal of Separation Science* **2021**, *44* (22), 4141–4150.
652 <https://doi.org/10.1002/jssc.202100528>.
- 653 (14) Scanlon, J. T.; Willis, D. E. Calculation of Flame Ionization Detector Relative Response Factors
654 Using the Effective Carbon Number Concept. *Journal of Chromatographic Science* **1985**, *23* (8),
655 333–340. <https://doi.org/10.1093/chromsci/23.8.333>.
- 656 (15) Liu, C.; Li, J.; Lin, Y. Optimization Study of Sub/Supercritical Water Liquefaction of Lignite: Fast
657 Liquefaction for High Bio-Oil Yield. *International Journal of Hydrogen Energy* **2019**, *44* (39),
658 21406–21412. <https://doi.org/10.1016/j.ijhydene.2019.06.140>.
- 659 (16) Audu, M.; Wang, H.; Arellano, D.; Cheng, F.; Dehghanizadeh, M.; Jarvis, J. M.; Yan, J.; Brewer, C.
660 E.; Jena, U. Ash-Pretreatment and Hydrothermal Liquefaction of Filamentous Algae Grown on
661 Dairy Wastewater. *Algal Research* **2021**, *57*, 102282.
662 <https://doi.org/10.1016/j.algal.2021.102282>.
- 663 (17) Chen, W.-T.; Qian, W.; Zhang, Y.; Mazur, Z.; Kuo, C.-T.; Scheppe, K.; Schideman, L. C.; Sharma,
664 B. K. Effect of Ash on Hydrothermal Liquefaction of High-Ash Content Algal Biomass. *Algal*
665 *Research* **2017**, *25*, 297–306. <https://doi.org/10.1016/j.algal.2017.05.010>.
- 666 (18) Liu, H.; Chen, Y.; Yang, H.; Gentili, F. G.; Söderlind, U.; Wang, X.; Zhang, W.; Chen, H. Conversion
667 of High-Ash Microalgae through Hydrothermal Liquefaction. *Sustainable Energy Fuels* **2020**, *4*
668 (6), 2782–2791. <https://doi.org/10.1039/C9SE01114E>.
- 669 (19) Liu, R.; Tian, W.; Kong, S.; Meng, Y.; Wang, H.; Zhang, J. Effects of Inorganic and Organic Acid
670 Pretreatments on the Hydrothermal Liquefaction of Municipal Secondary Sludge. *Energy*
671 *Conversion and Management* **2018**, *174*, 661–667.
672 <https://doi.org/10.1016/j.enconman.2018.08.058>.
- 673 (20) Shafizadeh, A.; Shahbeig, H.; Nadian, M. H.; Mobli, H.; Dowlati, M.; Gupta, V. K.; Peng, W.; Lam,
674 S. S.; Tabatabaei, M.; Aghbashlo, M. Machine Learning Predicts and Optimizes Hydrothermal
675 Liquefaction of Biomass. *Chemical Engineering Journal* **2022**, *445*, 136579.
676 <https://doi.org/10.1016/j.cej.2022.136579>.
- 677 (21) Oner, M.; Oner, G.; Bolat, E.; Yalin, G.; Kavlak, C.; Dincer, S. The Effect of Ash and Ash
678 Constituents on the Liquefaction Yield of Turkish Lignites and Asphaltites. *Fuel* **1994**, *73* (10),
679 1658–1666. [https://doi.org/10.1016/0016-2361\(94\)90147-3](https://doi.org/10.1016/0016-2361(94)90147-3).
- 680 (22) Vassilev, S. V.; Baxter, D.; Andersen, L. K.; Vassileva, C. G. An Overview of the Composition and
681 Application of Biomass Ash. Part 1. Phase–Mineral and Chemical Composition and
682 Classification. *Fuel* **2013**, *105*, 40–76. <https://doi.org/10.1016/j.fuel.2012.09.041>.
- 683 (23) Fedorova, N. I.; Ismagilov, Z. R. Ash Composition of Lignite. *Coke and Chemistry* **2019**, *62* (11),
684 493–497. <https://doi.org/10.3103/S1068364X19110036>.
- 685 (24) Prado, G. H. C.; Rao, Y.; de Klerk, A. Nitrogen Removal from Oil: A Review. *Energy Fuels* **2017**,
686 *31* (1), 14–36. <https://doi.org/10.1021/acs.energyfuels.6b02779>.
- 687 (25) Prado, G. H. C.; Rao, Y.; de Klerk, A. Nitrogen Removal from Oil: A Review. *Energy Fuels* **2017**,
688 *31* (1), 14–36. <https://doi.org/10.1021/acs.energyfuels.6b02779>.
- 689 (26) ASTM D7566-22 -Standard Specification for Aviation Turbine Fuel Containing Synthesized
690 Hydrocarbons. In *ASTM Volume 05.04: Petroleum Products, Liquid Fuels, And Lubricants (IV):*
691 *D7412 – D8128*; ASTM, 2023; Vol. 05.04, p 2074.

- 692 (27) Stefanova, M.; Marinov, S. P.; Magnier, C. Aliphatic Biomarkers from Miocene Lignites
693 Desulphurization. *Fuel* **1999**, *78* (12), 1395–1406. <https://doi.org/10.1016/S0016->
694 2361(99)00068-X.
- 695 (28) Liu, J.; Wei, X.-Y.; Zhang, D.-D.; Li, Z.-K.; Lv, J.-H.; Wang, T.-M.; Gui, J.; Qu, M.; Guo, L.-L.; Zong,
696 Z.-M.; Li, W.; Kong, L.-X. Characterization of Heteroatom-Containing Species in the Soluble
697 Portion from the Ethanolysis of the Extraction Residue from Xinghe Lignite by Electrospray
698 Ionization Fourier Transform Ion Cyclotron Resonance Mass Spectrometry. *Fuel* **2016**, *173*,
699 222–229. <https://doi.org/10.1016/j.fuel.2016.01.059>.
- 700 (29) Liu, P.; Zhang, D. Effect of Hydrothermal Treatment on the Carbon Structure of Inner Mongolia
701 Lignite. *International Journal of Coal Science & Technology* **2020**, *7* (3), 493–503.
702 <https://doi.org/10.1007/s40789-020-00356-7>.
- 703 (30) Shi, Z.; Jin, L.; Zhou, Y.; Li, Y.; Hu, H. Effect of Hydrothermal Treatment on Structure and
704 Liquefaction Behavior of Baiyinhua Coal. *Fuel Processing Technology* **2017**, *167*, 648–654.
705 <https://doi.org/10.1016/j.fuproc.2017.08.015>.
- 706 (31) Maes, I. I.; Gryglewicz, G.; Machnikowska, H.; Yperman, J.; Franco, D. V.; Mullens, J.; Van
707 Poucke, L. C. Rank Dependence of Organic Sulfur Functionalities in Coal. *Fuel* **1997**, *76* (5), 391–
708 396. [https://doi.org/10.1016/S0016-2361\(97\)85515-9](https://doi.org/10.1016/S0016-2361(97)85515-9).
- 709 (32) Patwardhan, P. R.; Timko, M. T.; Class, C. A.; Bonomi, R. E.; Kida, Y.; Hernandez, H. H.; Tester, J.
710 W.; Green, W. H. Supercritical Water Desulfurization of Organic Sulfides Is Consistent with
711 Free-Radical Kinetics. *Energy Fuels* **2013**, *27* (10), 6108–6117.
712 <https://doi.org/10.1021/ef401150w>.
- 713 (33) Meng, N.; Jiang, D.; Liu, Y.; Gao, Z.; Cao, Y.; Zhang, J.; Gu, J.; Han, Y. Sulfur Transformation in
714 Coal during Supercritical Water Gasification. *Fuel* **2016**, *186*, 394–404.
715 <https://doi.org/10.1016/j.fuel.2016.08.097>.
- 716 (34) Liao, J.; Fei, Y.; Marshall, M.; Chaffee, A. L.; Chang, L. Hydrothermal Dewatering of a Chinese
717 Lignite and Properties of the Solid Products. *Fuel* **2016**, *180*, 473–480.
718 <https://doi.org/10.1016/j.fuel.2016.04.027>.
- 719 (35) Liu, shucheng; Zhao, H.; Fan, T.; Zhou, J.; Liu, X.; Li, Y.; Zhao, G.; Wang, Y.; Zeng, M.
720 Investigation on Chemical Structure and Hydrocarbon Generation Potential of Lignite in the
721 Different Pretreatment Process. *Fuel* **2021**, *291*, 120205.
722 <https://doi.org/10.1016/j.fuel.2021.120205>.
- 723 (36) Calkins, W. H. The Chemical Forms of Sulfur in Coal: A Review. *Fuel* **1994**, *73* (4), 475–484.
724 [https://doi.org/10.1016/0016-2361\(94\)90028-0](https://doi.org/10.1016/0016-2361(94)90028-0).
- 725 (37) Fraga, G.; Batalha, N.; Kumar, A.; Bhaskar, T.; Konarova, M.; Perkins, G. Chapter 5 - Advances in
726 Liquefaction for the Production of Hydrocarbon Biofuels. In *Hydrocarbon Biorefinery*; Maity, S.
727 K., Gayen, K., Bhowmick, T. K., Eds.; Elsevier, 2022; pp 127–176. [https://doi.org/10.1016/B978-](https://doi.org/10.1016/B978-0-12-823306-1.00009-1)
728 0-12-823306-1.00009-1.
- 729 (38) Yan, S.; Xia, D.; Liu, X. Beneficial Migration of Sulfur Element during Scrap Tire
730 Depolymerization with Supercritical Water: A Molecular Dynamics and DFT Study. *Science of*
731 *The Total Environment* **2021**, *776*, 145835. <https://doi.org/10.1016/j.scitotenv.2021.145835>.
- 732 (39) Saturnino, D. Compréhension de la relation entre la structure physico-chimique et l'activité
733 des catalyseurs d'HDS vieillis, Université de Lyon, 2014.
- 734 (40) Zhu, C.; Gutiérrez, O. Y.; Santosa, D. M.; Kutnyakov, I.; Weindl, R.; Shi, H.; Wang, H. Impact of
735 Coprocessing Biocrude with Petroleum Stream on Hydrotreating Catalyst Stability. *Energy Fuels*
736 **2022**, *36* (16), 9133–9146. <https://doi.org/10.1021/acs.energyfuels.2c01748>.
- 737 (41) Benitez, A.; Ramirez, J.; Cruz-Reyes, J.; López Agudo, A. Effect of Alumina Fluoridation on
738 Hydroconversion Ofn-Heptane on Sulfided NiW/Al₂O₃Catalysts. *Journal of Catalysis* **1997**, *172*
739 (1), 137–145. <https://doi.org/10.1006/jcat.1997.1848>.
- 740 (42) WEISSER, O.; LANDA, S. 6 - HYDROGENATION, SYNTHESIS AND SOME REACTIONS OF
741 INDIVIDUAL ORGANIC COMPOUNDS IN THE PRESENCE OF SULPHIDE CATALYSTS. In *Sulphide*

- 742 *Catalysts, their Properties and Applications*; WEISSER, O., LANDA, S., Eds.; Pergamon, 1973; pp
743 118–284. <https://doi.org/10.1016/B978-0-08-017556-0.50011-3>.
- 744 (43) Girgis, M. J.; Gates, B. C. Reactivities, Reaction Networks, and Kinetics in High-Pressure
745 Catalytic Hydroprocessing. *Ind. Eng. Chem. Res.* **1991**, *30* (9), 2021–2058.
746 <https://doi.org/10.1021/ie00057a001>.
- 747 (44) Bello, S. S.; Wang, C.; Zhang, M.; Gao, H.; Han, Z.; Shi, L.; Su, F.; Xu, G. A Review on the Reaction
748 Mechanism of Hydrodesulfurization and Hydrodenitrogenation in Heavy Oil Upgrading. *Energy*
749 *Fuels* **2021**, *35* (14), 10998–11016. <https://doi.org/10.1021/acs.energyfuels.1c01015>.
- 750 (45) Xu, D.; Lin, G.; Guo, S.; Wang, S.; Guo, Y.; Jing, Z. Catalytic Hydrothermal Liquefaction of Algae
751 and Upgrading of Biocrude: A Critical Review. *Renewable and Sustainable Energy Reviews*
752 **2018**, *97*, 103–118. <https://doi.org/10.1016/j.rser.2018.08.042>.
- 753 (46) Cronin, D. J.; Subramaniam, S.; Brady, C.; Cooper, A.; Yang, Z.; Heyne, J.; Drennan, C.;
754 Ramasamy, K. K.; Thorson, M. R. Sustainable Aviation Fuel from Hydrothermal Liquefaction of
755 Wet Wastes. *Energies* **2022**, *15* (4), 1306. <https://doi.org/10.3390/en15041306>.
- 756 (47) Cooper, B. H.; Donnis, B. B. L. Aromatic Saturation of Distillates: An Overview. *Applied Catalysis*
757 *A: General* **1996**, *137* (2), 203–223. [https://doi.org/10.1016/0926-860X\(95\)00258-8](https://doi.org/10.1016/0926-860X(95)00258-8).
- 758 (48) Stanislaus, A.; Cooper, B. H. Aromatic Hydrogenation Catalysis: A Review. *Catalysis Reviews*
759 **1994**, *36* (1), 75–123. <https://doi.org/10.1080/01614949408013921>.
- 760 (49) Batalha, N.; Checa, R.; Lorentz, C.; Afanasiev, P.; Stańczyk, K.; Kapusta, K.; Laurenti, D.; Geantet,
761 C. Lignite and Biomass Waste Hydrothermal Liquefaction Crude Upgrading by Hydrotreatment.
762 *Energy Fuels* **2023**, *37* (14), 10506–10520. <https://doi.org/10.1021/acs.energyfuels.3c01550>.
- 763 (50) Korre, S. C.; Klein, M. T.; Quann, R. J. Polynuclear Aromatic Hydrocarbons Hydrogenation. 1.
764 Experimental Reaction Pathways and Kinetics. *Ind. Eng. Chem. Res.* **1995**, *34* (1), 101–117.
765 <https://doi.org/10.1021/ie00040a008>.
- 766 (51) Castello, D.; Haider, M. S.; Rosendahl, L. A. Catalytic Upgrading of Hydrothermal Liquefaction
767 Biocrudes: Different Challenges for Different Feedstocks. *Renewable Energy* **2019**, *141*, 420–
768 430. <https://doi.org/10.1016/j.renene.2019.04.003>.
- 769 (52) Sharma, K.; Castello, D.; Haider, M. S.; Pedersen, T. H.; Rosendahl, L. A. Continuous Co-
770 Processing of HTL Bio-Oil with Renewable Feed for Drop-in Biofuels Production for Sustainable
771 Refinery Processes. *Fuel* **2021**, *306*, 121579. <https://doi.org/10.1016/j.fuel.2021.121579>.
- 772 (53) Subramaniam, S.; Santosa, D. M.; Brady, C.; Swita, M.; Ramasamy, K. K.; Thorson, M. R.
773 Extended Catalyst Lifetime Testing for HTL Biocrude Hydrotreating to Produce Fuel Blendstocks
774 from Wet Wastes. *ACS Sustainable Chem. Eng.* **2021**, *9* (38), 12825–12832.
775 <https://doi.org/10.1021/acssuschemeng.1c02743>.
- 776 (54) da Costa Magalhães, B.; Checa, R.; Lorentz, C.; Afanasiev, P.; Laurenti, D.; Geantet, C. Catalytic
777 Hydroconversion of HTL Micro-Algal Bio-Oil into Biofuel over NiWS/Al₂O₃. *Algal Research*
778 **2023**, *71*, 103012. <https://doi.org/10.1016/j.algal.2023.103012>.
- 779 (55) Magalhães, B. C.; Checa, R.; Lorentz, C.; Prévot, M.; Afanasiev, P.; Laurenti, D.; Geantet, C.
780 Catalytic Hydrotreatment of Algal HTL Bio-Oil over Phosphide, Nitride, and Sulfide Catalysts.
781 *ChemCatChem* **2023**, *15* (9), e202300025. <https://doi.org/10.1002/cctc.202300025>.
- 782 (56) Nagappan, S.; Bhosale, R. R.; Nguyen, D. D.; Chi, N. T. L.; Ponnusamy, V. K.; Woong, C. S.;
783 Kumar, G. Catalytic Hydrothermal Liquefaction of Biomass into Bio-Oils and Other Value-Added
784 Products – A Review. *Fuel* **2021**, *285*, 119053. <https://doi.org/10.1016/j.fuel.2020.119053>.
- 785 (57) Watson, J.; Wang, T.; Si, B.; Chen, W.-T.; Aierzhati, A.; Zhang, Y. Valorization of Hydrothermal
786 Liquefaction Aqueous Phase: Pathways towards Commercial Viability. *Progress in Energy and*
787 *Combustion Science* **2020**, *77*, 100819. <https://doi.org/10.1016/j.pecs.2019.100819>.
- 788 (58) Wang, B.; Huang, Y.; Zhang, J. Hydrothermal Liquefaction of Lignite, Wheat Straw and Plastic
789 Waste in Sub-Critical Water for Oil: Product Distribution. *Journal of Analytical and Applied*
790 *Pyrolysis* **2014**, *110*, 382–389. <https://doi.org/10.1016/j.jaap.2014.10.004>.

- 791 (59) Shen, Y.; Wu, H.; Pan, Z. Co-Liquefaction of Coal and Polypropylene or Polystyrene in Hot
792 Compressed Water at 360–430°C. *Fuel Processing Technology* **2012**, *104*, 281–286.
793 <https://doi.org/10.1016/j.fuproc.2012.05.023>.
- 794 (60) Channiwala, S. A.; Parikh, P. P. A Unified Correlation for Estimating HHV of Solid, Liquid and
795 Gaseous Fuels. *Fuel* **2002**, *81* (8), 1051–1063. [https://doi.org/10.1016/S0016-2361\(01\)00131-4](https://doi.org/10.1016/S0016-2361(01)00131-4).
- 796 (61) Verdier, S.; Mante, O. D.; Hansen, A. B.; Poulsen, K. G.; Christensen, J. H.; Ammtizboll, N.;
797 Gabrielsen, J.; Dayton, D. C. Pilot-Scale Hydrotreating of Catalytic Fast Pyrolysis Biocrudes:
798 Process Performance and Product Analysis. *Sustainable Energy Fuels* **2021**, *5* (18), 4668–4679.
799 <https://doi.org/10.1039/D1SE00540E>.
- 800 (62) Song, C.; Ma, X. New Design Approaches to Ultra-Clean Diesel Fuels by Deep Desulfurization
801 and Deep Dearomatization. *Applied Catalysis B: Environmental* **2003**, *41* (1), 207–238.
802 [https://doi.org/10.1016/S0926-3373\(02\)00212-6](https://doi.org/10.1016/S0926-3373(02)00212-6).
- 803 (63) Hao, B.; Xu, D.; Jiang, G.; Sabri, T. A.; Jing, Z.; Guo, Y. Chemical Reactions in the Hydrothermal
804 Liquefaction of Biomass and in the Catalytic Hydrogenation Upgrading of Biocrude. *Green*
805 *Chem.* **2021**, *23* (4), 1562–1583. <https://doi.org/10.1039/D0GC02893B>.
806